JOURNAL OF GEOPHYSICAL RESEARCH, VOL. 96, NO. C5, PAGES 8517–8529, MAY 15, 1991

Climatological Perspectives, Oceanographic and Meteorological, on Variability in the Subtropical Convergence Zone in the Northwestern Atlantic

HOWARD P. HANSON

Cooperative Institute for Research in Environmental Sciences, University of Colorado at Boulder

PETER CORNILLON, GEORGE R. HALLIWELL, JR.,[1] AND VICKI HALLIWELL[1]

Graduate School of Oceanography, University of Rhode Island, Narragansett

We discuss the large-scale setting for the Frontal Air-Sea Interaction Experiment (FASINEX). A climatology of the west-central North Atlantic, derived from various data sets, is presented, and the meteorological and oceanographic context for FASINEX is thereby established. While the atmospheric and oceanic processes of interest during the intensive phases of FASINEX are not resolved in this large-scale study, we are able to show how these scales produce an environment favorable to the smaller-scale processes of frontogenesis that are the subject of other contributions in this issue.

1. INTRODUCTION

The Frontal Air-Sea Interaction Experiment (FASINEX) was designed specifically to focus on the atmospheric and oceanic dynamics and thermodynamics within the vicinity of sea-surface temperature (SST) fronts and how the presence of these fronts modifies air-sea interaction processes [*Weller*, this issue]. The research aircraft flight plans, for example, included extensive mapping on scales of tens of kilometers, and the oceanographic analog (the SEASOAR surveys) was also conducted on this spatial scale [*Friehe et al.*, this issue; *Eriksen et al.*, this issue]. The fronts of interest are the results of large-scale and mesoscale processes that produce SST gradients of up to 0.3°C km^{-1} [*Halliwell et al.*, this issue; *Weller et al.*, this issue]. The large-scale climatological environment that is favorable to this frontal activity is the topic of this paper.

Such strong fronts are not observed everywhere in the oceans. Based on previous oceanographic surveys showing considerable frontal activity in the area [e.g., *Voorhis et al.*, 1976], the Sargasso Sea southwest of Bermuda was chosen for FASINEX research. The time of year chosen for the intensive phases, January–March, was thought to be a time during which the SST signatures would be clearly visible with satellite sensors (SST gradients are washed out by surface heating during the summer months), and this was the case, as the papers in this series will show. However, we will also show that the large-scale processes that set up the favorable environment for frontal activity are not limited to the winter months.

1.1. Historical Background

The average large-scale circulation of the central North Atlantic, between about 15° and 45°N, has long been known to consist of a basin-scale anticyclonic gyre. The earliest hint of a unified description of this dates back to *Halley* [1688]. Physical oceanography textbooks that discuss the history of the development of circulation theory point to Benjamin Franklin's description of the Gulf Stream system as a significant contribution [e.g., *Neumann and Pierson*, 1966], and the southward (northward) course taken by westward (eastward) bound shipping is steeped in tradition as well as practicality. The west-central part of the gyre, the Sargasso Sea, held a reputation in the early days of sail as a graveyard for ships: even today, this myth persists as the legendary "Bermuda Triangle." Although observations of windrows of seaweed and other debris in this part of the gyre have been made by mariners since the very beginnings of the exploration of the oceans, it was not until *Ekman* [1905] introduced the concept of a balance between the Coriolis acceleration and friction that a simple theoretical explanation for the implied convergence was available. Even now, more than 80 years later, a complete theoretical explanation for the scales of the convergence has yet to be determined.

Ekman theory provides a basis for the discussions in this paper of the large-scale convergence in the Sargasso Sea, but details of frontal circulations observed during FASINEX require more sophisticated analyses. The convergence on large scales (O(10^3) km), averaged over months, provides the background environment in which the smaller-scale processes leading to frontogenesis, studied during the intensive field phases of the experiment, take place. In this paper, we begin the discussion of FASINEX results by concentrating on the largest scales. Subsequent contributions in this issue will focus on increasingly smaller scales.

This telescoping of observational results is parallel to a telescoping of physical processes. The gross features of the gyre (southward drift with return flow on the western boundary) are described by Sverdrupian dynamics. Details of westward intensification of the return flow(that is, the formation of the Gulf

[1] Now at Division of Meteorology and Physical Oceanography, Rosenstiel School of Marine and Atmospheric Science, University of Miami, Miami, Florida.

Paper number 90JC02487.
0148-0227/91/90JC-02487$05.00

Stream) require the introduction of friction and the variation of the Coriolis parameter with latitude [*Stommel*, 1948]. Ekman theory involves internal friction and ocean-atmosphere coupling; the large-scale mean wind pattern produces a meridional convergence of Ekman transport (and hence downwelling) within the gyre. Consequently, the central portion of the gyre is often referred to as the subtropical convergence zone. Since the meridional direction is nearly normal to the mean surface isotherms, this wind pattern acts to increase the magnitude of the SST gradients within a zonally oriented band several degrees wide. This band is typically found between 25° and 32°N in the Sargasso Sea [*Halliwell and Cornillon*, 1990*a*,*b*]. Smaller-scale, nonlinear dynamical processes operating within this band then act to form the strong fronts found there. This paper focuses solely on the large-scale climatology of the SST and SST gradient fields, along with the large-scale climatology of surface atmospheric forcing fields. *Halliwell et al.* [this issue] focus both on the mesoscale (O(10^2) km) and the large-scale variability of these fields during FASINEX (January through June 1986), relating the observed properties of these fields at large scales to the observed climatology described here. *Davidson et al.* [this issue] focus on the large-scale meteorological variability during FASINEX.

1.2. Overview

We discuss here a 40-year climatology of the FASINEX area using the Comprehensive Ocean-Atmosphere Data Set (COADS) [*Woodruff et al.*, 1987] and somewhat higher resolution, shorter-term climatologies constructed from the National Ocean Data Center (NODC) archives. The COADS data include a number of derived parameters as well as the (processed) observations, and allow the larger scales of Ekman convergence in the area to be assessed. With the NODC data, we begin the process of analyzing increasingly smaller scales of variability over a time interval of decreasing length that is converging toward the 6-month FASINEX interval.

We begin with a discussion of surface marine observations of SST and its variability, both annual and interannual. The marine meteorology of the FASINEX area is then discussed in terms of the surface pressure and winds, the sea-air temperature difference, and the cloud cover. This is followed by an oceanographic climatology, derived from the NODC archives, that describes upper ocean currents and density structure.

2. Sea Surface Temperature

2.1. COADS Background

The COADS consists of a compilation of surface marine observations from all available sources; for practical purposes, the usable data begin in the mid-1800s. The data set has been culled for duplicate and obviously erroneous observations, and the products used for the climatology discussed here were monthly averaged over 2° squares. *Woodruff et al.* [1987] discuss the data processing; further details are given by *Slutz et al.* [1985]. For the analyses that follow, we have used data from 1948 to 1987 for the long-term climatology. Data coverage, particularly for the quantities used here in the smaller averaging domain described below, is quite good for this period. In the cases where data was missing for a given month (this occurred mostly for COADS squares in the far northeast of the large domain in Figure 1), the long-term monthly mean was substituted.

We present long-term averages of observed quantities in a 32° square box centered approximately on the FASINEX site, shown as the triangle in Figure 1. Variability analyses involve the 12° square box inset in Figure 1, this in order to confine the analyses to the central part of the subtropical gyre, away from the influence of the Gulf Stream. All presentations of derived quantities are confined to the 12° domain. The 2° resolution of the COADS product used here is indicated by the tic marks around the edges of Figure 1. It is worth noting that the compositing used in this COADS product defines as "ocean" 2° squares that are mostly continental (for example, in the Florida panhandle and central Maine). These data bias the results below in the vicinity of coasts in two ways: first, coastal data are not necessarily representative of open-ocean conditions in neighboring squares (thus introducing strong gradients near the coast); second, the data points are implicitly moved, by the analysis, to the centers of the squares (thus shifting the location of the data in the analysis). The 2° averaging also causes COADS not to recognize as land significant geographic regions (for example, Nova Scotia, the Florida peninsula, and the Caribbean islands of Cuba and Hispaniola). Because the FASINEX area is well offshore, however, these effects do not bias the results below in that region. Other aspects of COADS data inhomogeneity have been discussed by *Ramage* [1984, 1987] and *Wright* [1986]. The analysis here benefits from the relatively data-rich area in the North Atlantic used and the recent decades chosen to produce the climatology.

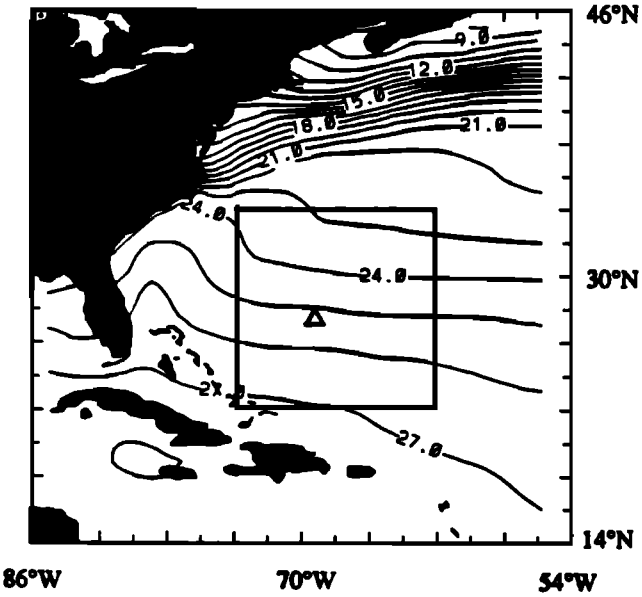

Fig. 1. The 40-year average of SST (in degrees Celsius) in the northwestern subtropical Atlantic from COADS. The inset box shows the area used for the annual and interannual analyses; the triangle indicates the position of the FASINEX moored array.

2.2. SST Climatology

Long-term average. Figure 1 shows the long-term average SST (the 40-year annual average) for the 32° square domain. As expected, horizontal variability in the SST signal in the western North Atlantic is dominated by the Gulf Stream. However, the zonally oriented large-scale frontal band expected to be found in the subtropical convergence zone is visually evident. It is confined approximately between the 24° and 26°C isotherms (between about 25° and 30°N) within the 12° box. In the FASINEX area the annually averaged temperature is about 3°C warmer than the temperatures during the intensive measurement phase, which was

conducted near the time of the seasonal SST minimum (see below). The smoothing implicit in this long-term average eliminates any transient features such as Gulf Stream rings. These do, however, appear in individual monthly maps [e.g., *Davidson et al.*, this issue].

The stationarity of the 40-year record was tested by dividing it into two 20-year segments, each of which was then separately averaged. The differences in these averages (not shown) indicate little long-term trend, the two fields being within less than 1°C of each other over the entire analysis domain. Slightly positive values occur north of the Gulf Stream and negative values (indicating that the years 1968–1987 were cooler than 1948–1967) occur off the coast of the Carolinas. A domain-wide average of the differences yields a net cooling of less than 0.01°C, which is insignificant, especially considering the obvious coastal influences.

Annual variability. The annual variability of the SST in the smaller 12° domain inset in Figure 1 is summarized in Figure 2*a* with (top) the spatial pattern and (bottom) time series of the first empirical orthogonal eigenfunction (EOF) of the averaged monthly averages (that is, the time series of 40 averaged Januaries, 40 averaged Februaries, etc.). This EOF explains over 99% of the variance of the departures of these averaged monthly averages from the annual average shown in Figure 1. This and subsequent EOF patterns will be interpreted in terms of nondimensional values of the spatial patterns and dimensional values of the time series; thus the vertical scale of the time series in Figure 2*a* ranges from -4° to 5°C. (The EOFs shown in this paper were obtained using the covariance matrix of the relevant data set and a least squares regression fit for the time series, and hence they resolve patterns of standing fluctuations in the maps.) For reference, the location of the FASINEX moored array is shown in the upper panels of Figure 2 at the triangle.

Except in the northwest corner of the 12° domain, the dominant signal in the annual cycle is a zonally symmetric, N–S movement of isotherms. Note that for the FASINEX array in an average February, the SST is about 3°C lower than the annual average SST, or about 22.5°C. This is about 1°C lower than the temperatures observed in the array during FASINEX Phase II [*Weller et al.*, this issue]. Therefore 1986 was a warm year in this area. These warm temperatures were also observed in the satellite data [*Halliwell and Cornillon*, 1990*a*].

The amplitude of the annual cycle is higher in the northern part of the domain than in the south. This implies that the large-scale, N–S SST gradient decreases during the summer and increases during the winter. The relatively strong large-scale frontal band between about 25° and 30°N virtually disappears in summer. During this season the strongest meridional gradients in the Sargasso Sea are found north of 30°N [see *Halliwell et al.*, this issue]. Maximum gradients occur in late February. Because the minimum gradients occur in early August, at the time of the highest SSTs, the heating phase is slightly shorter than the cooling phase of the annual cycle. This is consistent with the slightly higher amplitude of the time series in August than in February.

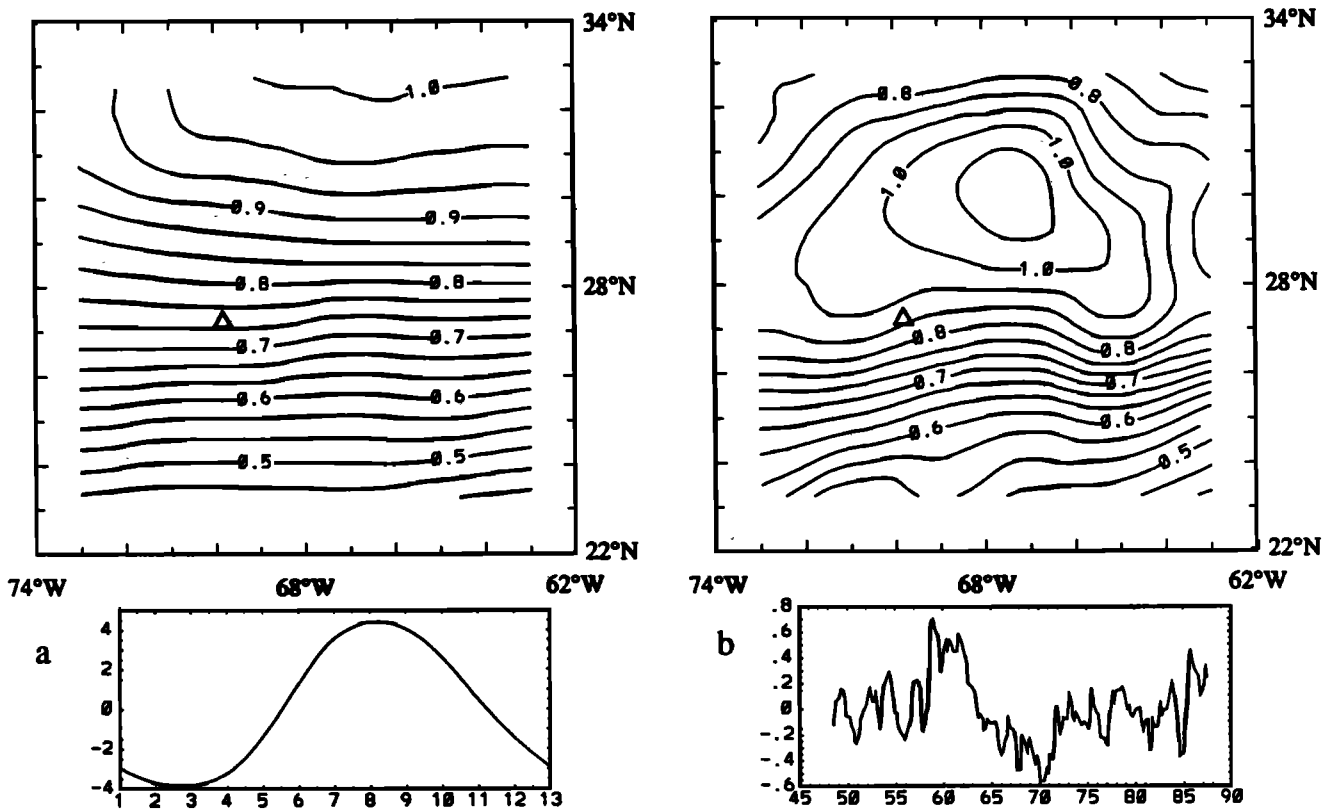

Fig. 2. (*a*) Annual variability of the SST in the 12° analysis domain as represented by the first EOF of averaged monthly averages (that is, the monthly mean field: 40 Januaries, 40 Februaries, etc., with the annual average subtracted out). (Top) The spatial pattern (the superimposed triangle shows the position of the FASINEX array) is dimensionless; (bottom) the time series has the dimension of temperature (in degrees Celsius). The product of these represents 99% of the annual variance. (*b*) Interannual variability of the SST in the 12° domain as represented by the first EOF of the field of individual monthly departures from the long-term mean and averaged annual cycles. This EOF accounts for 46% of the interannual variance.

Interannual variability. The dominant mode of interannual variability of the SST in the 12° domain is shown in Figure 2*b*. This is the first EOF of the monthly departures from the two previous data sets; that is, the annual average and averaged monthly departures have been subtracted out. This EOF represents an in-phase interannual oscillation of SST that is largest in the northern half of the domain. The largest magnitude is centered near 30°N, 67.5°W. The isotherm pattern is nearly zonally oriented to the south of about 27.5°N, and hence to the south of the FASINEX moored array. This EOF represents about 46% of the variance of the time series. Note the nearly order-of-magnitude decrease in the amplitude of the variability, compared to the annual cycle. The time series exhibits variations on the 2- to 5-year scale, but there are no obvious correlations with other, global scale variability. For example, the significant El Niño/Southern Oscillation events of 1972 and 1982 are not apparent. The February 1986 contribution of this EOF in the area of the FASINEX moored array is about 0.4°C; this shows that 1986 was an anomalously warm year in the area. In fact, for the entire 40-year record, only the period 1959–1962 was warmer than FASINEX. Moreover, FASINEX followed directly an anomalously cold year, 1985.

In years where the time series is positive (negative), the meridional SST gradient is weaker (stronger) than usual between 24° and 27.5°N. Thus during periods such as the early 1960s and the FASINEX measurement period, the large-scale frontal band may have been weaker or may have been displaced farther to the north than average. During periods such as the late 1960s / early 1970s and the 2 years prior to FASINEX, it may have been weaker or may have been displaced farther to the south than average. This hypothesis is partly supported by the satellite observations presented by *Halliwell and Cornillon* [1990*b*], who observed that the strongest meridional SST gradients existed near 27.5°N during winter 1983–1984, near 28.5°N during winter 1984–1985, and near 29.5°N during winter 1985–1986 (FASINEX). Also, the magnitude of this gradient was about 20% smaller during winter 1985–1986 than during the previous two winters. To some extent, the strength and location of the frontal band are correlated (negatively for strength and positively for latitude) with the average magnitude of the SST anomaly within the 12° box.

2.3. SST Gradient

Despite the relatively smooth appearance of the SST contours in the long-term average of the FASINEX area of interest (Figure 1), SST fronts are commonly observed there, as other articles in this issue will describe. It is the averaging scales of COADS, monthly and ~200 km, that smooth the fronts in this analysis. Nevertheless, there is evidence that this area is favorable to frontal formation. This can be seen from the magnitude of the SST gradient (Figures 3*a* and 3*b*) and in the Ekman pumping by the windstress (see section 3).

For this paper the SST gradient was computed using fully centered differences on the 12° analysis domain. (As can be inferred from Figure 1, the gradient pattern for the larger-scale domain would be dominated by the Gulf Stream.) The long-term average of the magnitude of the SST gradient (Figure 3*a*) reveals a ridge of maximum gradient across the middle of the area at 30°N. This is intensified and shifted slightly southward during winter (Figure 3*b*), so that the FASINEX array was located approximately at the latitude of maximum gradient in February and March. During summer the entire pattern relaxes, but there remains a zone of maximum gradient toward the north of the 12° domain, as can be inferred from Figures 3*a* and 3*b*. These results are to be compared to the Ekman pumping patterns shown in the next section.

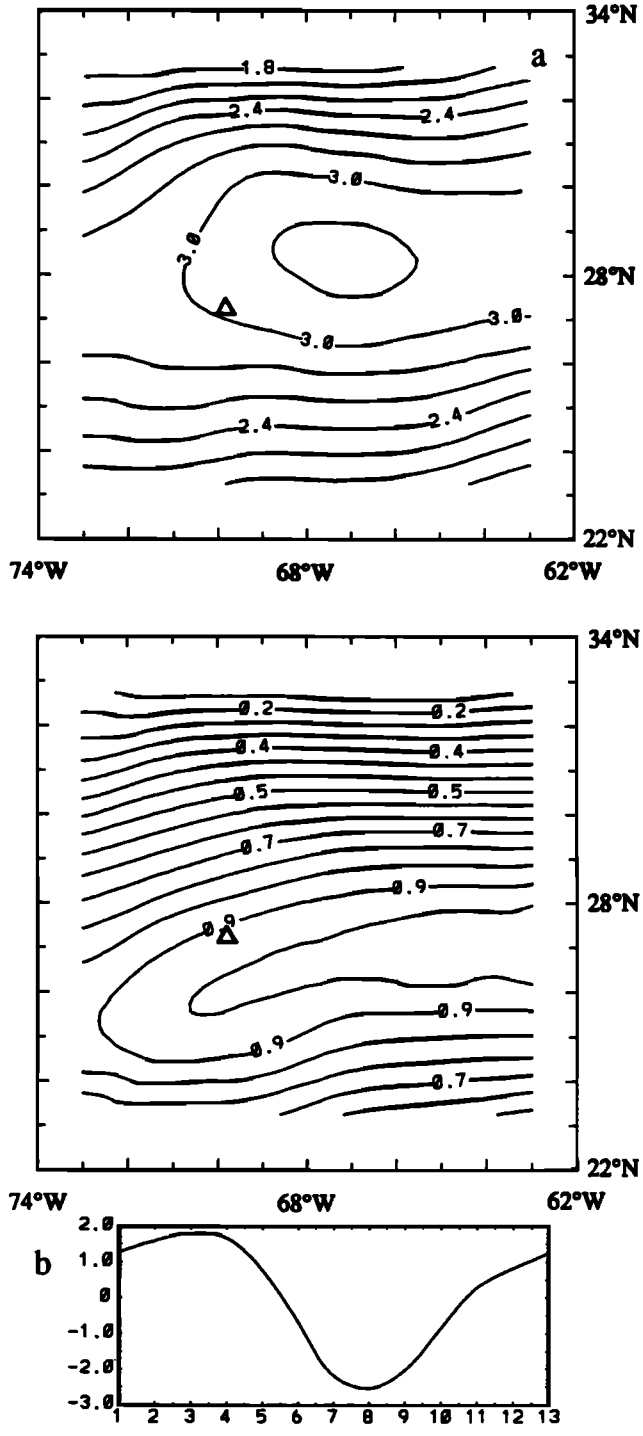

Fig. 3. (*a*) The 40-year average of the magnitude of the SST gradient in the 12° analysis domain. Units (on the time series) are 10^{-5} °C m^{-1} (note that 0.9 × 10^{-5} °C m^{-1} – 1 °C (° latitude)$^{-1}$). (*b*) First EOF of the monthly mean field of the magnitude of the SST gradient, representing 97% of the annual variance.

3. Lower Atmosphere

3.1. Surface Pressure and Winds

Figure 4 presents the 40-year average of the surface pressure field, with wind vectors superimposed, for the 32° square domain. The pressure field is dominated by the subtropical high, the axis of which passes (in the annual average) about 2° north of the FASINEX array. The wind patterns exhibit the belt of westerlies

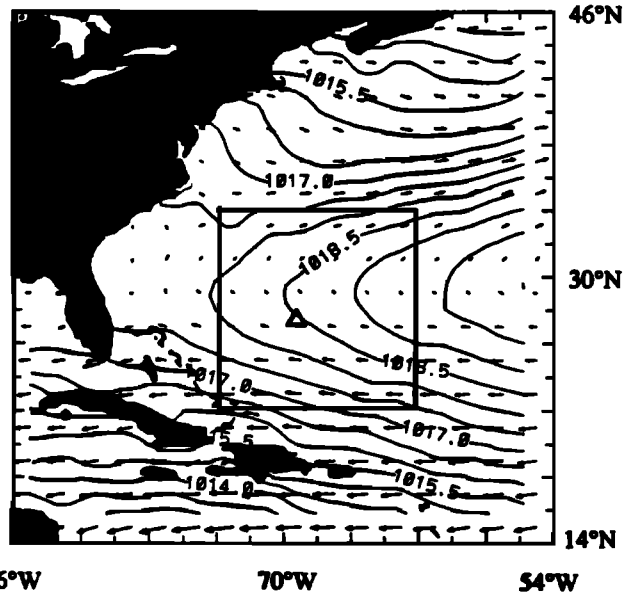

Fig. 4. The 40-year average of surface pressure (hPa) and wind vectors (the distance between tic marks represents a vector of 10 m s^{-1}) in the northwestern subtropical Atlantic.

to the north, and the trade winds to the south, of the subtropical high. The flow becomes more geostrophically balanced toward the north.

The annual variability of the pressure field (for which the first EOF in Figure 5*a* explains 87% of the variance) is more complex than the behavior of the SST. For most of the year (mid-November to mid-August), the spatial pattern reinforces the subtropical high with a slight displacement southward. During winter and spring, this contribution is quite weak, with maximum pressure changes of order 1 hPa. During the summer months, however, this southward displacement is also associated with a strengthening of the subtropical high. (This behavior is emphasized in the individual monthly maps; see *Davidson et al.* [this issue]). There is then an abrupt switchover to a weaker subtropical high during the fall.

The interannual variability of the surface pressure field (Figure 5*b*) exhibits predominately zonal behavior, with stronger variations to the north. The first EOF in Figure 5*b* explains 71% of the variance, so this is a truly dominant mode. In terms of the surface pressure, 1986 was a "normal" year, as can be seen from the time series. As with the SST, there is no obvious correlation of this time series with other large-scale modes of variability.

It can be seen from Figure 4 that there is a large-scale Ekman convergence, associated with the westerlies to the north of the 12° domain and the easterly trades to the south, centered approximately on the FASINEX area. This is confirmed by Ekman pumping calculations (Figure 6). For these, drag coefficients dependent on wind speed and sea-air temperature difference [*Smith*, 1988] were used with centered differences. The long-term average (Figure 6*a*) is everywhere negative (that is, downward motion) and relatively flat, with variations of about 20% of the mean of less than about 10 cm d^{-1}. The downward pumping peaks in winter (Figure 6*b*), at which time the values are approximately doubled in the northern part of the domain and enhanced by 20–30% in the southern part. At the site of the FASINEX moorings, the averaged February Ekman pumping is about -1.5×10^{-9} m s^{-1}. During summer, the Ekman pumping decreases dramatically, but there is never upwelling in the domain.

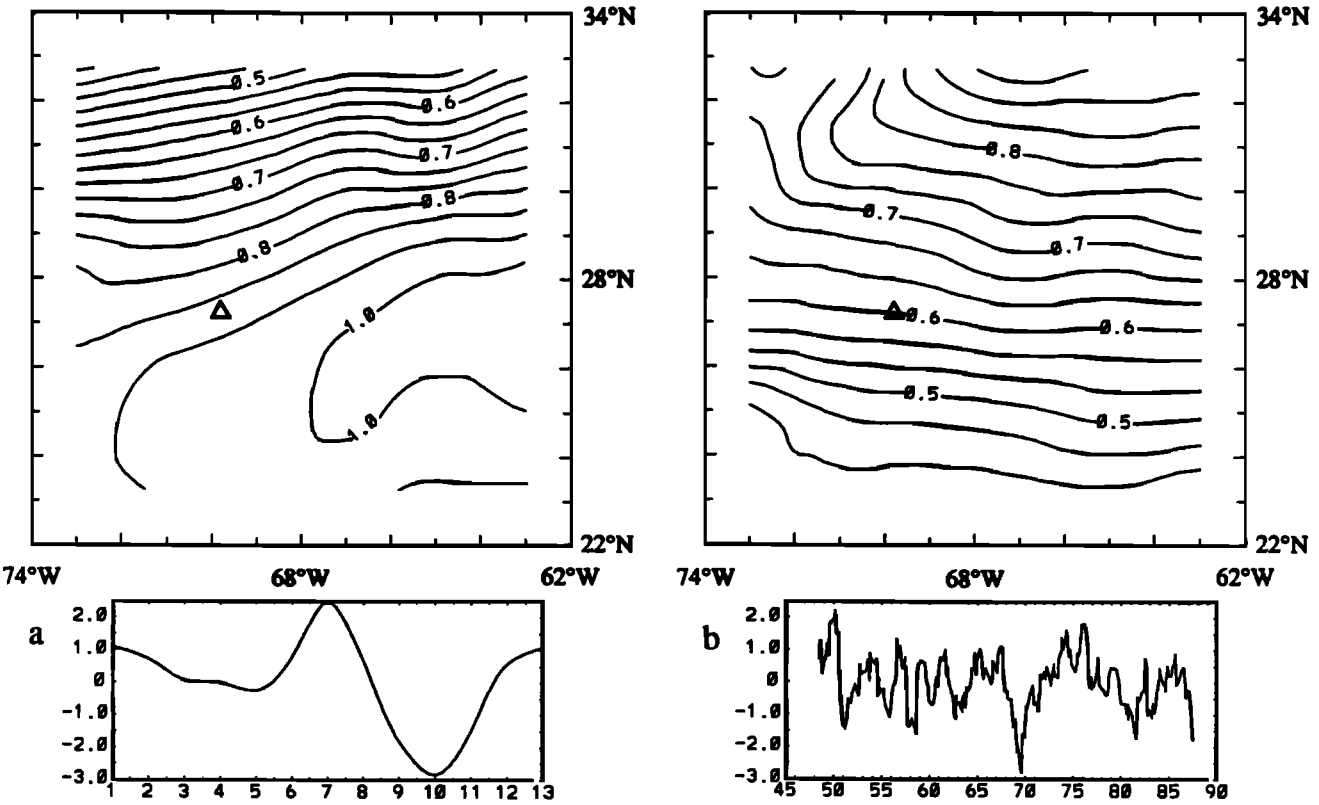

Fig. 5. (*a*) First EOF of the monthly mean surface pressure field, representing 87% of the annual variance. (*b*) First EOF of the 40-year field of monthly departures of surface pressure, representing 71% of the interannual variance.

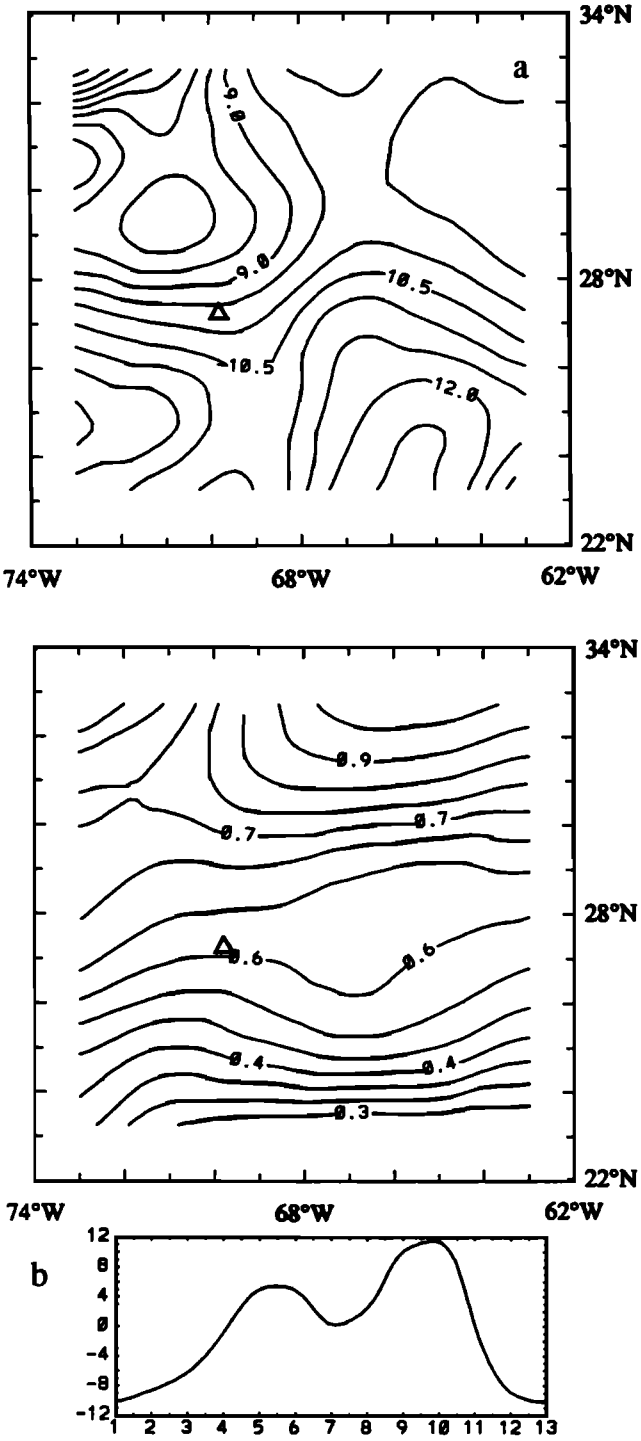

Fig. 6. (*a*) The 40-year average of Ekman pumping velocity in the 12° domain. Negative values indicate downward motion, in units of 10^{-7} m s^{-1} (note that -11.6×10^{-7} m s^{-1} ~ -10 cm d^{-1}). (*b*) First EOF of the monthly mean field of Ekman pumping, representing 66% of the annual variance.

Because most of the Ekman pumping is associated with the curl of the zonal wind stress (that is, $-\partial\tau_x/\partial y$), the implied convergence can be related to the SST gradients depicted in Figure 3. The relatively flat field of downward pumping in the mean suggests that water from north and south of the domain will converge in a ridge, concentrating gradients there (Figure 3*a*), and the approximately out-of-phase seasonal cycles of the gradient and the pumping are also consistent (Figures 3*b* and 6*b*). However, it is clear that there are other processes at work on the SST field. Other papers in this issue discuss smaller-scale processes; we conclude this section of this large-scale analysis with a brief discussion of thermodynamic influences on the SST.

3.2. *Sea-Air Temperature Difference*

Energy exchange between ocean and atmosphere, including both thermal and mechanical energy, is one focus of FASINEX. Therefore the conditions that affect the efficiency of this transfer are an important component of the FASINEX environment. In order to summarize those conditions, we present here a climatological analysis of the sea-air temperature difference, $\Delta T_{SA} = T_S - T_A$.

Of the several quantities that determine air-sea energy exchange, including not only ΔT_{SA} but also the wind speed, the atmospheric humidity, and the radiative fluxes, ΔT_{SA} variability is the most revealing. The stability of the atmospheric surface layer, and thus the magnitude of the drag and transfer coefficients, is determined largely by ΔT_{SA}; the sensible heat flux is, of course, proportional to ΔT_{SA}. The latent heat flux, in the FASINEX area, is also controlled by ΔT_{SA} because the atmospheric relative humidity is nearly constant (for monthly averages) at ~80 ± 5%. Further, in the 12° averaging domain used here, the wind speed hovers within about 1.5 m s^{-1} of 6 m s^{-1} in the annual average; the seasonal variability is also about ±1.5 m s^{-1}, with maximum wind speeds in the late winter in the northern part of the 12° analysis domain. The averaged total (sensible plus latent) heat flux in the FASINEX area is 195 W m^{-2} in February, compared to 160 W m^{-2} annually. Bowen ratios are much larger in winter (~0.14) than in the summer (~ 0.03), reflecting the seasonality of the sea-air temperature difference and the increased evaporation in summer when the SST is larger.

Figure 7 shows the 40-year average of sea-air temperature difference ΔT_{SA} (in degrees Celsius), as derived from COADS. The influence of the Gulf Stream and the North Atlantic Current is obvious, with a region of high ΔT_{SA} covering the northwest corner of the 12° analysis domain. In the area of the FASINEX array, ΔT_{SA} is approximately 1°C on average.

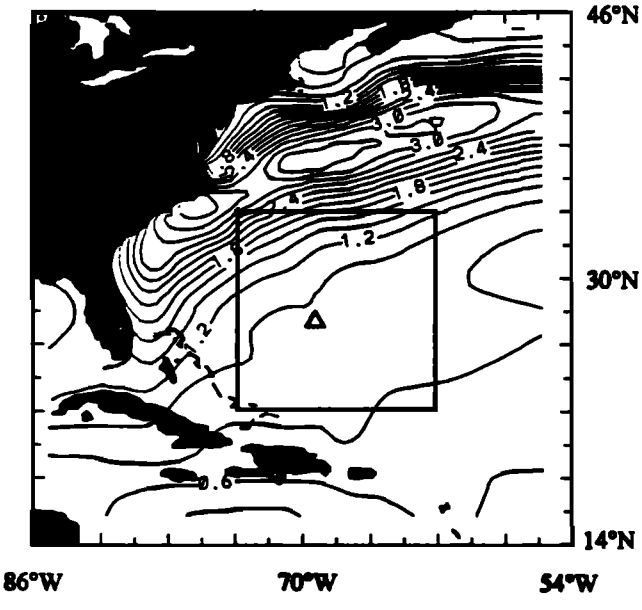

Fig. 7. The 40-year average of sea-air temperature difference ΔT_{SA} (in degrees Celsius) in the northwestern subtropical Atlantic.

The annual variability of ΔT_{SA}, for which the first EOF in Figure 8*a* represents 98% of the variance, exhibits a similar spatial pattern to the average in Figure 7. Consequently, the annual cycle acts to enhance and decrease the ΔT_{SA} gradient most strongly in the northwest corner of the domain and to increase and decrease ΔT_{SA} everywhere. This behavior is clearly associated with annual variability of the Gulf Stream system. The maximum ΔT_{SA} occurs in early December, and the minimum occurs in June (this is considerably earlier in the year than the maximum SST, however). The climatological ΔT_{SA} in the FASINEX array, in February, is about 1.5°C.

Unlike the interannual variability of the SST and the surface pressure, the first EOF of the interannual ΔT_{SA} represents only 36% of the variance. However, because the second EOF represents a considerably lower amount (7.5%), the first EOF (shown in Figure 8*b*) is significant. The pattern is similar to the average and annual cycle, and, as with most other quantities, the amplitude is considerably lower. Beyond the apparent power in the 2- to 5-year range, there is no obvious correlation with other variables. This is not unexpected, due to the influence of continental air masses moving off North America over the region of interest.

3.3. Cloud Cover

We conclude our analysis of the marine meteorological climate of the FASINEX region with a presentation of cloud cover. The cloud cover observations in COADS are total cloud cover, so that these statistics are not readily comparable to the discussions of clouds observed in the marine boundary layer during FASINEX. However, because of the importance of clouds to the global energy budget, as well as to their role in obscuring satellite observations of SST fronts, they represent an important aspect of the FASINEX environment. The study by *Warren et al.* [1988] of the different types of clouds observed over the ocean indicates that the most frequently occurring types of clouds in the FASINEX area in February are stratus and stratocumulus, followed closely by altostratus and altocumulus. This is consistent with the observations made during the experiment.

The 40-year average (in tenths, Figure 9) shows a predominantly zonal pattern over much of the area of interest, with cloudiness increasing toward the north. In the FASINEX array, the average is just over 40% cover. The first EOF of the annual variability (Figure 10*a*), which represents 75% of the variance, acts to enhance and decrease the N–S gradient of cloud cover, with the minimum occurring in July. The climatological cloudiness in February near the FASINEX array averages about 70%. As with ΔT_{SA}, the interannual variability of cloud cover, as represented by the first EOF (Figure 10*b*), explains a relatively small (33%) amount of the variance, but, compared to other EOFs, it is significant. The pattern shows a ridge of maximum variability just to the north of the FASINEX array; the degree to which this may be associated with interannual variability of the frontal zone is unknown. The time series in Figure 10*b* indicates that, while 1986 was a relatively normal year, there is a hint of an overall trend toward increasing cloud cover in the area; in this context, the cloud cover during the intensive phase of FASINEX was 10–20% greater than the long-term average.

4. Upper Ocean

4.1. Annual Averages

Owing to data limitations, development of a climatology of the upper ocean is considerably more problematic than that for the sea surface or the marine atmosphere. We have used data from the

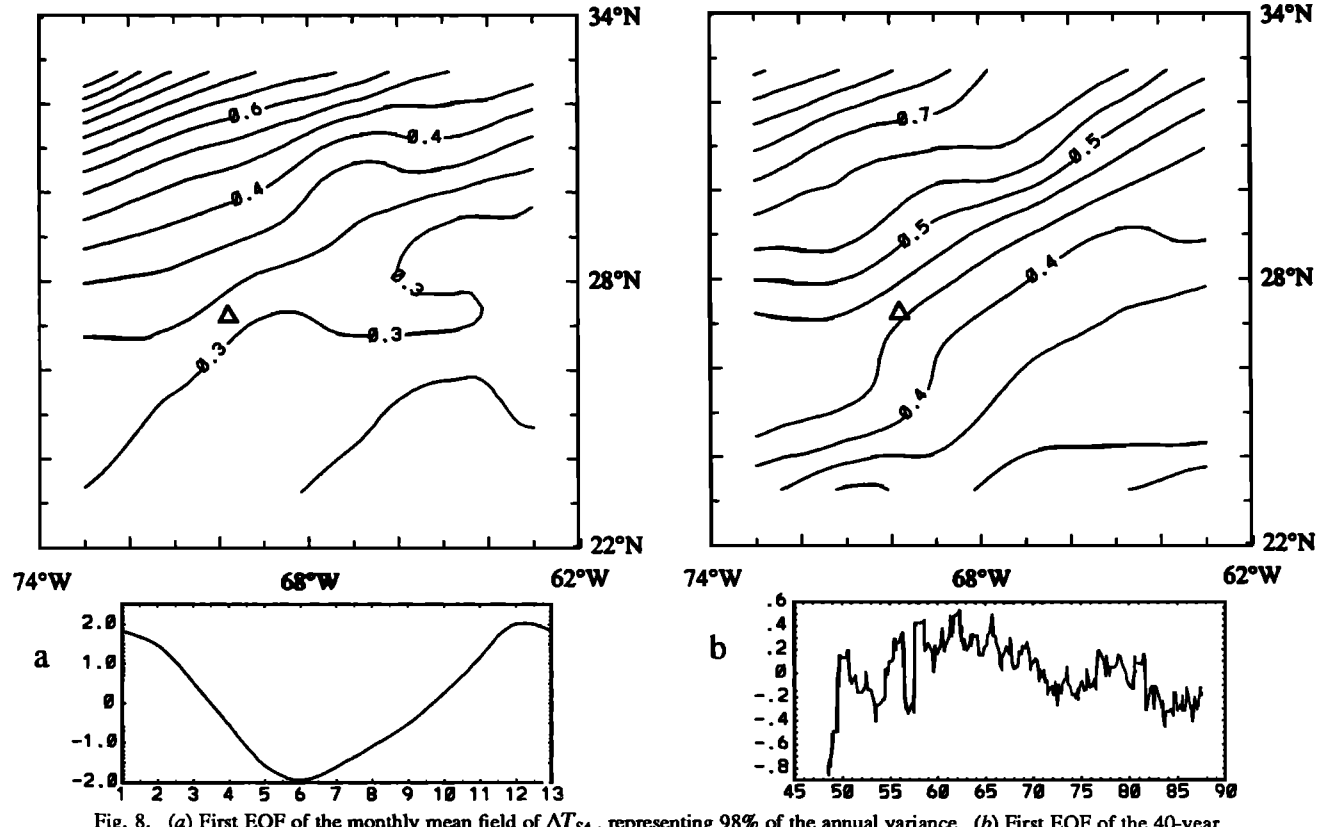

Fig. 8. (*a*) First EOF of the monthly mean field of ΔT_{SA}, representing 98% of the annual variance. (*b*) First EOF of the 40-year field of monthly departures of ΔT_{SA}, representing 36% of the interannual variance.

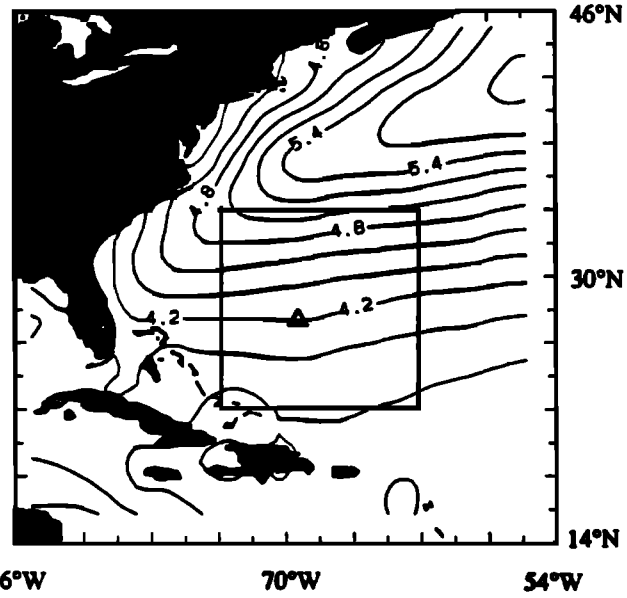

Fig. 9. The 40-year average of total cloud cover (tenths) in the northwestern subtropical Atlantic.

NODC archive as described ny the *Levitus* [1982] climatological atlas to analyze subsurface conditions in the 12° analysis domain in the vicinity of the FASINEX array. All expendable bathythermograph and mechanical bathythermograph data used by Levitus, plus the conductivity-temperature-depth, salinity-temperature-depth and Nansen casts, in the area 22°–34°N, 62°–74°W were composited by season for the analyses below. As with the atmospheric and surface climatologies, the resulting subsurface climatology represents features as considerably smoothed compared to the observations presented in other papers in this issue. However, this climatology establishes the long-term averaged environment in which the smaller-scale processes of frontogenesis observed during the intensive phases occur.

Figure 11 shows cross sections of the long-term, annual average potential temperature, salinity, potential density, and zonal geostrophic current (relative to 1500 m), zonally averaged across the 12° analysis domain, for the upper 1000 m. There is a very smoothed seasonal thermocline above about 250 m. Between about 250 m and 1000 m, isotherms and isohalines slope upward to the north; that is, at a given depth, both the temperature and the salinity decrease toward the north. The temperature field thus tends to increase the density northward, while the salinity tends to decrease northward. Since the isopycnals mimic the isotherms (sloping upward to the north), it can be seen that salinity compensation is not a strong factor in this layer. Below the salinity minimum (and flat temperature field) at about 1000 m, isotherms, isohalines, and isopycnals all slope downward to the north (not shown).

The zonal current structure is, at the surface, eastward everywhere, with a maximum at about 25°N and a minimum at about 30°N. The eastward currents extend to about 500 m, with a weak westward flow below. There is little evidence of horizontal shear near the surface, where the frontal zone is found. The broad eastward current maximum near 25°N is probably the Sargasso Sea analog of the eastward subtropical countercurrent described by Japanese researchers [e.g., *Uda and Hasunuma,* 1969; *Yoshida and Kidokoro,* 1967]. However, the eastward flow at all latitudes between 22° and 34°N is very surprising because westward near-surface flow along the southern part of the subtropical gyre is expected both north and south of the subtropical countercurrent.

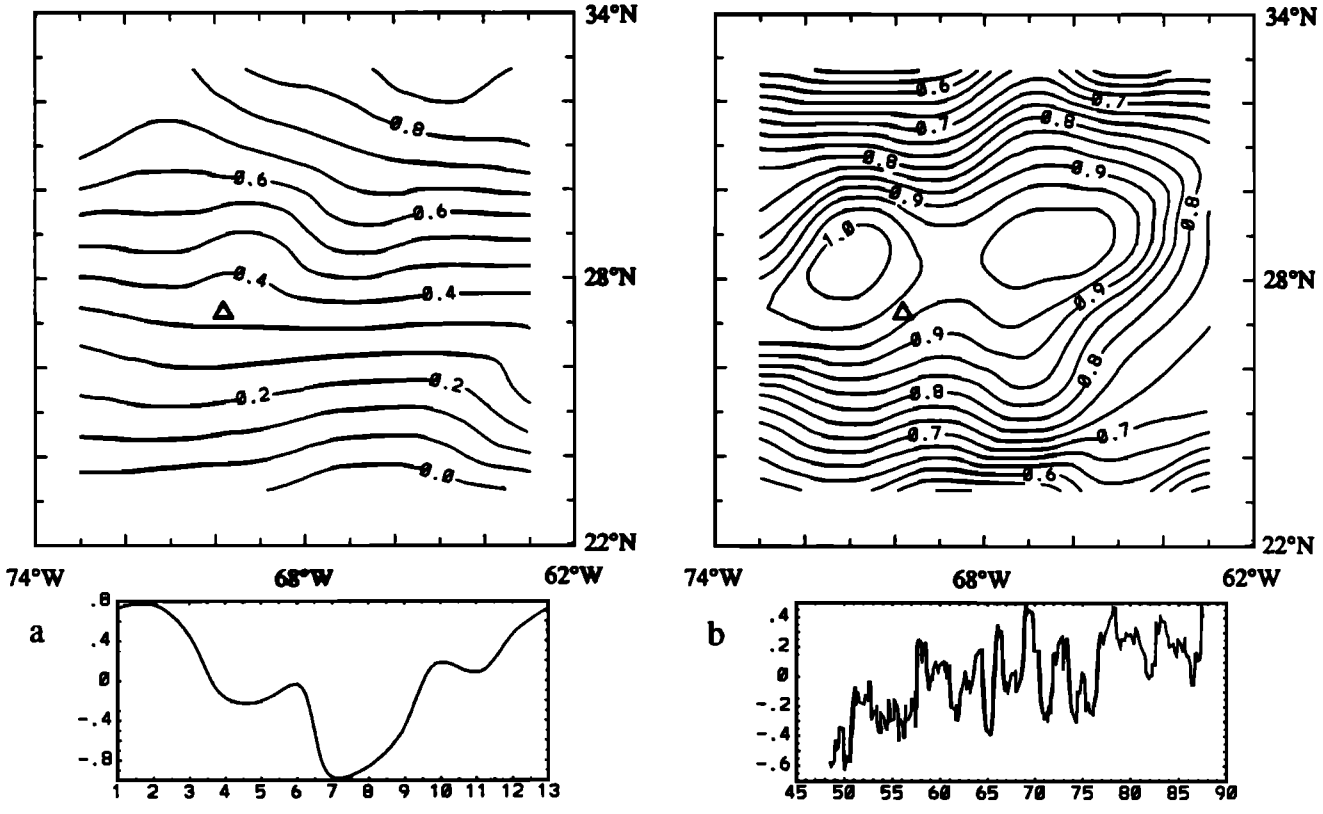

Fig. 10. (*a*) First EOF of the monthly mean field of total cloud cover, representing 75% of the annual variance. (*b*) First EOF of the 40-year time series of monthly departures of cloud cover, representing 33% of the interannual variance.

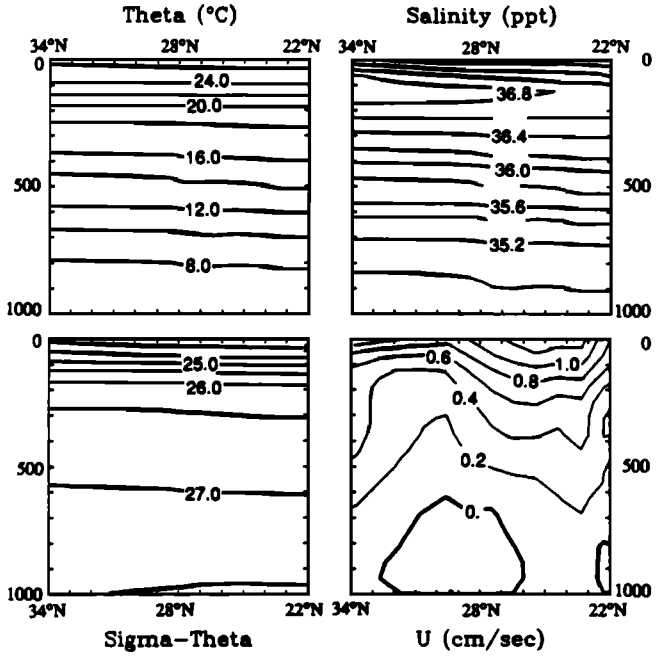

Fig. 11. Annual averages, zonally averaged across the 12° domain, of potential temperature, salinity, potential density and zonal geostrophic current for the top 1000 m.

Inspection of the meridional temperature cross sections presented by *Schroeder* [1965] indicates that from 22°N to about 28°–30°N, isotherms tend to shoal toward the north as we observe here. To the north of 28°–30°N, isotherms tend to deepen toward the north, reaching their maximum depth near 36°–37°N, the latitude where Subtropical Mode Water is often formed in late winter. This dip in the isotherms may also be associated with the Gulf Stream recirculation cell. Unfortunately, this isotherm depression north of 28°–30°N is not reproduced in the Levitus data, possibly due in part to the extreme smoothness of these fields. The relative change of zonal velocity with latitude, in particular the existence of the subtropical countercurrent, is more accurately represented than the absolute velocity.

4.2. *Seasonal Averages*

Seasonal averages, shown in Figures 12, reveal considerably more detail, although below about 250 m (the approximate base of the seasonal thermocline), differences with the annual average are small. In winter (Figure 12*a*), there is a strong well-mixed layer to about 100 m with generally higher salinity, and there is a hint of a layer of minimum vertical temperature gradient below the seasonal thermocline. The geostrophic current structure is similar to that of the annual average. Note that the horizontal shear at the surface is also substantially stronger that the annual average. In spring (Figure 12*b*), the surface layers have begun warm substantially and the minimum surface salinity has shifted northward; this combination changes the density structure and the associated currents dramatically.

The summertime patterns (Figure 12*c*) show the effects of strong surface heating and relatively uniform evaporation: the surface salinity minimum is uniform and the mixed layer is much warmer and shallower than that in winter. By fall (Figure 12*d*), the transition toward the winter pattern has begun, with a deeper, cooler mixed layer, a shift of the salinity minimum southward, and the beginnings of the winter–spring current structure.

4.3. *Upper Oceanic Structure*

The archived NODC data were used to determine the depth of the seasonal thermocline and to calculate the vertically integrated heat content and total potential energy in the water from the surface to this depth. For each cast, the top of the seasonal thermocline was obtained in an upward looking search beginning at the shallower of (1) the depth where the water temperature falls below 18°C, or (2) 400 m. The depth of maximum Brunt-Väisälä frequency (N) above this level was selected as the middle of the seasonal thermocline (neglecting the top 10 m to avoid diurnal effects). The top of the seasonal thermocline was chosen to be the depth at which N falls below $1/e$ of its maximum value. The vertically integrated heat content and total potential energy were then calculated from:

$$H = \int_z^0 c_p T \rho \, dz \quad ; \quad P = \int_z^0 g \rho \, z \, dz \, ,$$

where c_p and g are the specific heat of water and gravitational acceleration, respectively. For the 20-year annual and seasonal means, the three parameters were binned and averaged over 2° squares and contoured. The fields of both heat content and potential energy resemble the mixed layer depth, so further analysis was performed only on the mixed layer depth. Because all fields exhibited a high degree of zonal consistency, yearly and seasonal zonal averages for each year were also calculated for the mixed layer depth.

The long-term (20-year) mean mixed layer depth (Figure 13*a*) shows that the mixed layer is shallower in the region where the fronts are usually found and that the mixed layer is deeper both to the north and south of this latitude band. As noted before, the pattern is distinctly zonal, with the shallowest mixed layer at any latitude occurring at about 28°N. This is consistent with the mean wind (and consequently, wind stress) pattern over the area (Figure 4). The stronger wind to the north (the westerlies) and to the south (the easterly trade winds) of the study area should force deeper mixed layers than in the central portion, the transition zone between the westerlies and the trade winds. There also seems to be a slight zonal gradient in the wind speed at the latitude of minimum speed, which may be responsible for the shoaling of the mixed layer toward the east at 28°N. Shallower mixed layers have been observed in the vicinity of oceanic fronts, such as the subtropical front, regardless of the wind pattern. Numerical simulations of a convergent frontal region also show such a tendency [*Cushman-Roisin*, 1981].

The patterns of heat content (Figure 13*b*) and total potential energy (Figure 13*c*) are both similar to the mixed layer depth, as would be expected. The minimum in both heat content and potential energy is coincident with that of the mixed layer. However, note that the heat content is somewhat larger in the southern portion of the study area, since the water is warmer to the south than it is in the northern portion. Conversely, the potential energy maximum occurs toward the north of the frontal region owing to the deeper, relatively cold mixed layers there.

The seasonally averaged mixed layer depth (Figure 14*a*), heat content (Figure 14*b*) and potential energy (Figure 14*c*) all behave generally as expected. There is strong deepening in winter, when the mixed layer is deeper than 80 m everywhere, and is deeper than 150 m in the extreme northern part of the study area. In both spring and fall, there are rather strong horizontal (primarily meridional) gradients in mixed layer depth, whereas in summer the mixed layer is not only shallowest, but also somewhat more uniform over the domain. The deeper winter mixed layer results in

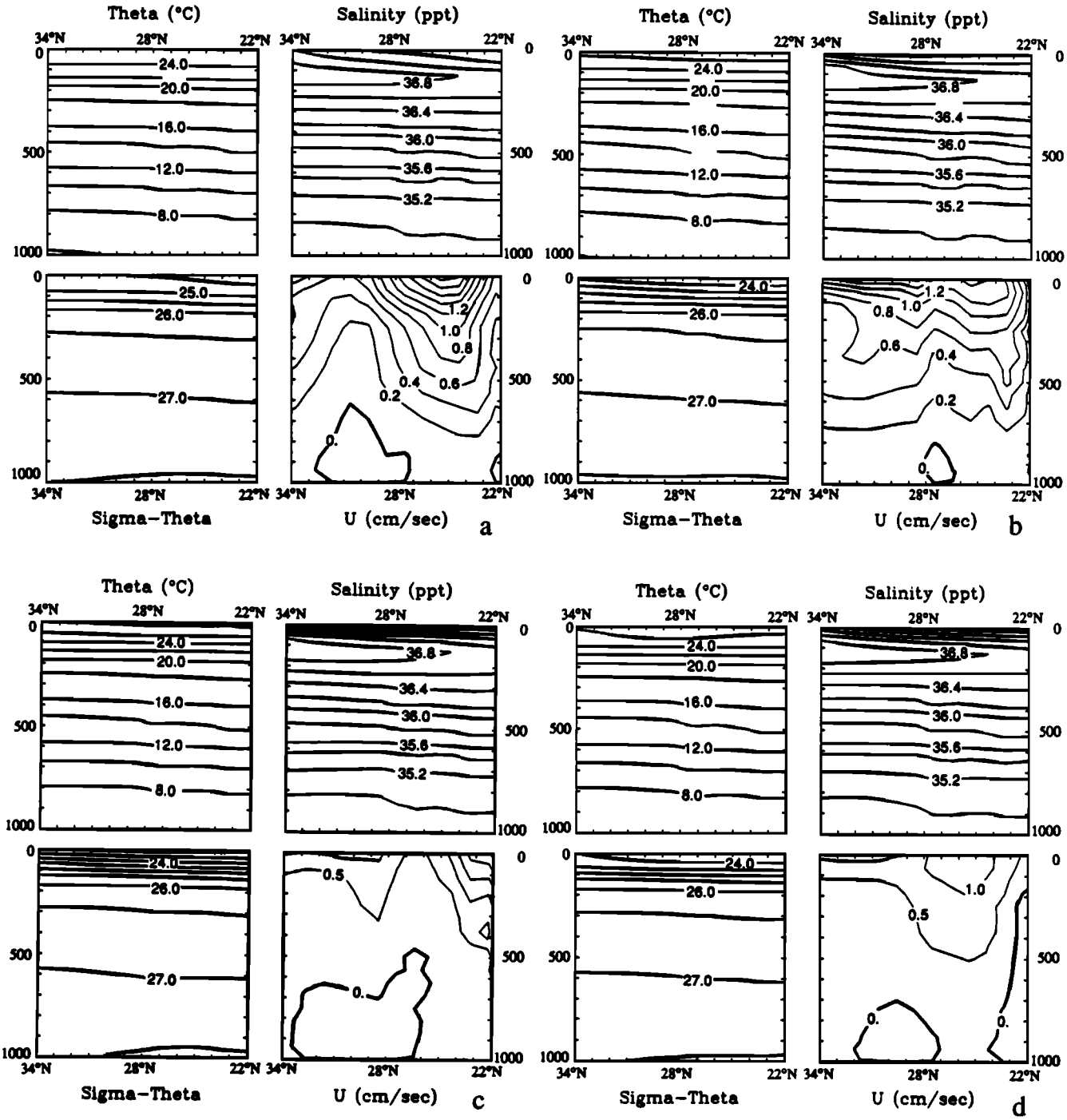

Fig. 12. Same as in Figure 11, except for (*a*) winter (December–February); (*b*) spring (March–May); (*c*) summer (June–August); and (*d*) fall (September-November).

both heat content and potential energy that is nearly twice as large as in spring and fall, and much larger than in summer (nearly an order of magnitude in the case of the potential energy). Thus while the ocean is substantially warmer in the summer, the heat content is dominated by the mixed layer depth.

In an attempt to isolate interannual variability, the mixed layer depth was averaged zonally over 2° of latitude for each year (Figure 15) and also seasonally (Figure 16). The yearly average (Figure 15) shows that for the most part, the shallowest mixed layer occurs around 28°N. The seasonal zonal averages (Figure 16) for all 20 years show a distinct seasonal cycle, with a winter deepening that is strongest to the north occurring most years. Note, however, that while for most years the winter mixed layer is deeper than 120 m, for a period of time in the early and mid-1970s (1970–1977) the winter mixed layer was shallower than 120 m. Another anomalous year occurred in 1985, the year before the FASINEX experiment. While the winter mixed layer did deepen below 150 m, the maximum depths were displaced south to the middle of the study area (that is, where the shallowest layers normally occur).

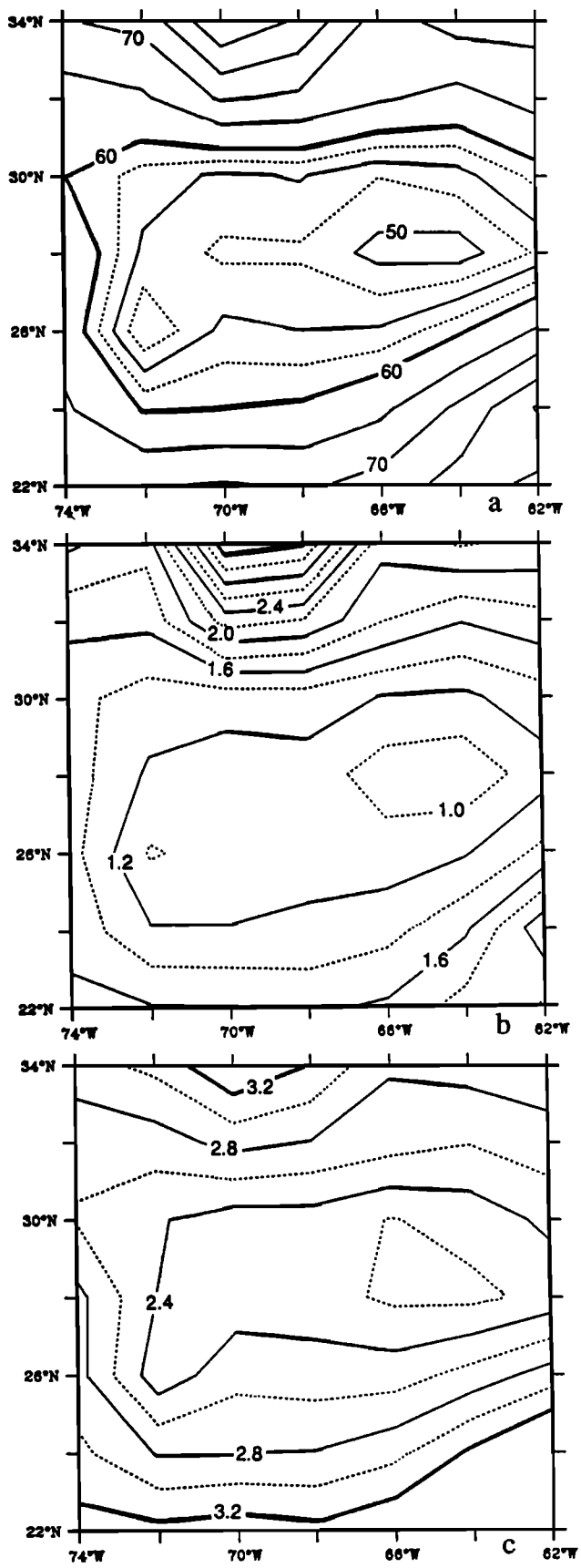

Fig. 13. The 20-year mean mixed layer depth (in meters) (*a*); (*b*) vertically integrated heat content H of the mixed layer (10^5 kJ m $^{-2}$); and (*c*) mean vertically integrated total potential energy P of the mixed layer (10^3 kJ m^{-2}).

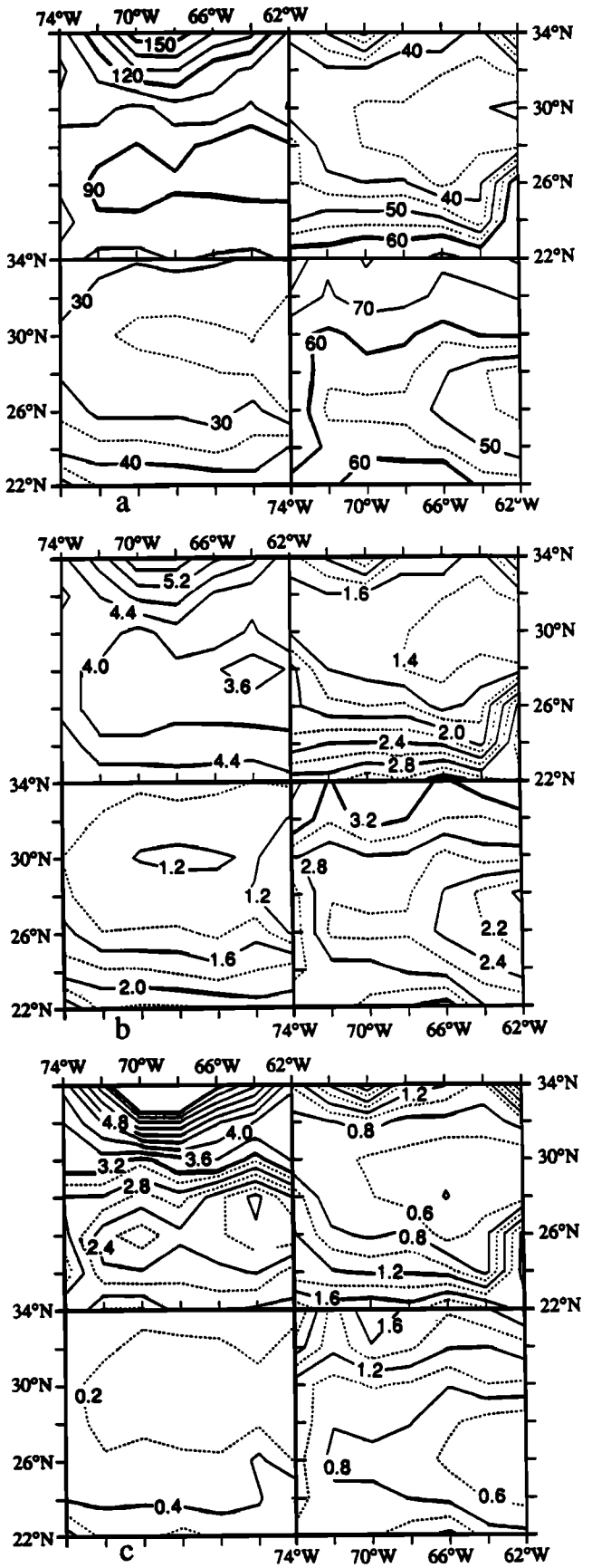

Fig. 14. Seasonal mixed layer depth (in meters) (*a*); (*b*) vertically integrated heat content H of the mixed layer (10^5 kJ m^{-2}); and (*c*) vertically integrated total potential energy P of the mixed layer (10^3 kJ m^{-2}). Seasons are as in Figure 12.

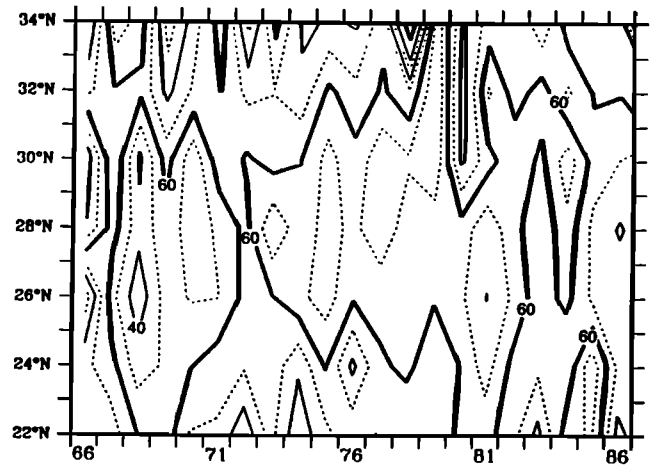

Fig. 15. Yearly zonal average mixed layer depth (in meters).

5. Summary and Conclusions

We have presented the large-scale, long-term climatology of lower atmosphere and upper ocean for the northwestern subtropical Atlantic, with emphasis on the FASINEX area. Both long-term and annual variability were discussed (data permitting), and the context for the FASINEX has thus been established.

On the time and space scales discussed here, the large-scale setting for the FASINEX is dominated by the subtropical high and its seasonal variability. In February, near 28°N in the western North Atlantic, the western end of the ridge of the subtropical high extends over the FASINEX area, and there is averaged southerly flow in the lower atmosphere. Conditions in 1986 were fairly typical, but the high was shifted slightly southward, with a concomitant tendency for mean westerly flow. This location relative to the high, on average, produces conditions favorable for convergence, and hence frontal formation and downwelling, in the upper ocean. However, based on the 2° spatial and monthly temporal averages presented here, evidence for frontal formation is limited to a tendency for a maximized SST gradient in the region. No evidence for the intense fronts observed during the FASINEX intensive period is seen on these scales. Of course, the monthly averaging completely smooths the strong forcing of synoptic systems that pass through the area.

Also missing on these averaging scales is evidence for frontal influence on the surface heat budget and/or on cloudiness. The Feburary averaged total heat flux of just under 200 W m^{-2} is dominated by the latent heat flux, but there is a significant sensible heat flux (~25 W m^{-2}) as well. The cloud cover is dominated by low- and mid-level stratus and shallow cumulus, with the mean cloud cover close to 50%.

The timing and position of the intensive measurement periods of FASINEX appears, from these results, to have been as nearly

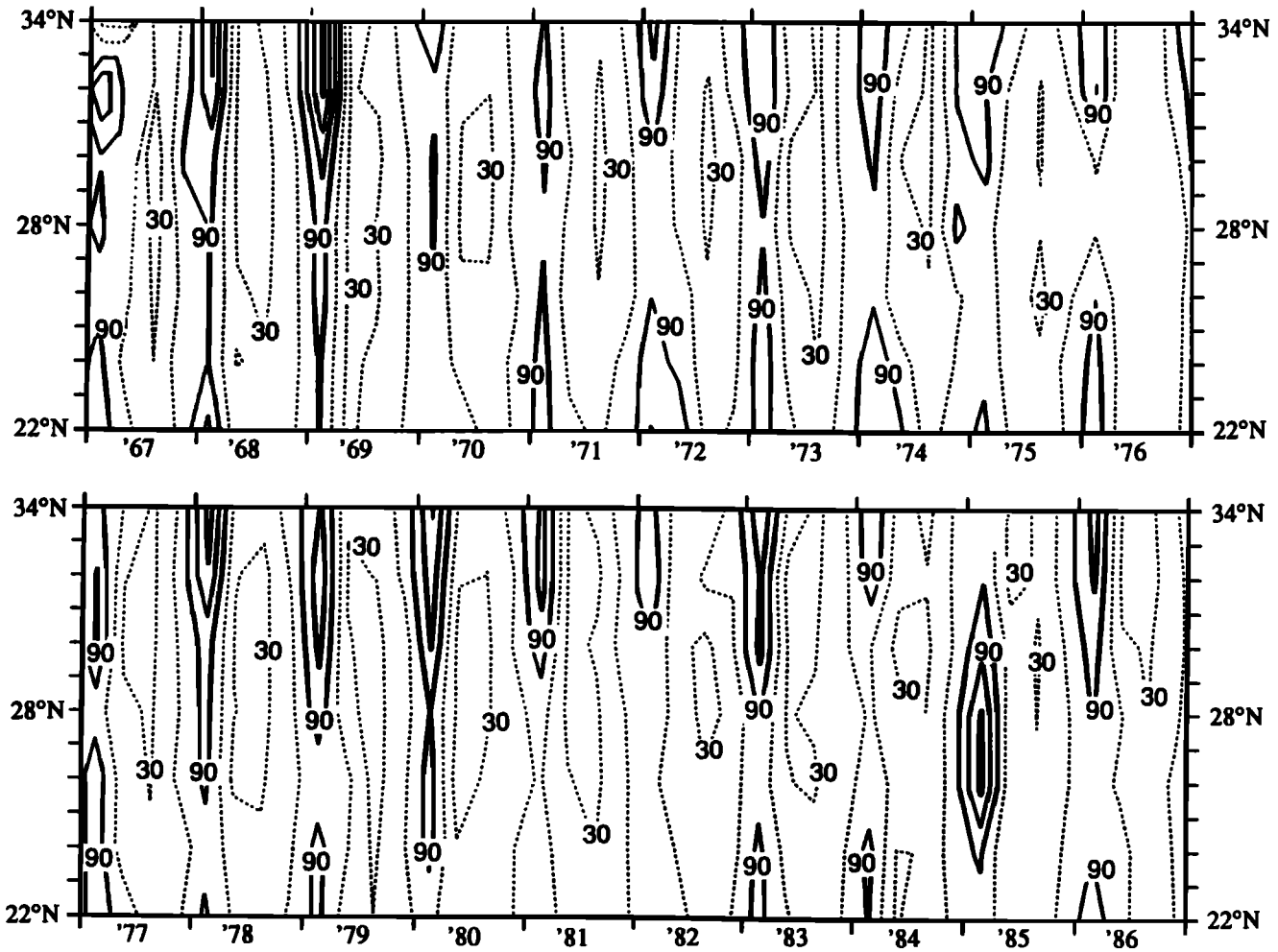

Fig. 16. Seasonal zonal average mixed layer depth, 1966–1986. The 30- and 60-m contours are dashed, 90-, 120-, 150- and 180-m contours are solid.

as optimal as possible, given observed variability. In particular, near 28°N in February is a favorable time and place to observe large mean temperature gradients and downward Ekman pumping. There is, meanwhile, a relatively smooth field of air-sea fluxes in the vicinity, so that oceanic forcing is dominated by large-scale processes. Further, 1986 seems not to have been an anomalous year, compared to the 40-year mean.

Of course, these results are highly smoothed versions of the observations made during FASINEX, and details of frontal structure and air-sea interaction processes in the vicinity of the front are not resolved here. Other contributions to this issue will address these smaller scales. Our intention has been to provide the setting in which these more detailed analyses reside.

Acknowledgments. We are pleased to acknowledge the following sources of support for this research: Contract N000-14-84-K-0405 from the Office of Naval Research and Grant DE-FG02-90ER61019 from the Department of Energy to the University of Colorado, and Contract N00014-87-KT0235 from the Office of Naval Research and Grant 957627 from the National Aeronautics and Space Administration to the University of Rhode Island.

REFERENCES

Cushman-Roisin, B., Effects of horizontal advection on upper ocean mixing: A case of frontogenesis, *J. Phys. Oceanogr., 11,* 1345–1356, 1981.

Davidson, K. D., P. J. Boyle, C. Gautier, H. P. Hanson, and S. J. S. Khalsa, Medium- to large-scale variability. during the Frontal Air-Sea Interaction Experiment, *J. Geophys. Res.,* this issue.

Ekman, V. W., On the influence of the earth's rotation on ocean currents, *Arch. Math. Astron. Phys., 2,* 1–53, 1905.

Eriksen, C. C., R. A. Weller, D. L. Rudnick, R. T. Pollard, and L.A. Regier, Ocean frontal variability in the Frontal Air-Sea Interaction Experiment, *J. Geophys. Res.,* this issue.

Friehe, C. A., W. J. Shaw, D. P. Rogers, K. L. Davidson, W. G. Large, S. A. Stage, G. H. Cresenti, and F. Li, Air-sea fluxes and surface layer turbulence around a sea surface temperature front, *J. Geophys. Res.,* this issue.

Halley, E., An historical account of the trade winds and monsoon observable in the seas between and near the tropics, *Philos. Trans., 16,* 153–168, 1688.

Halliwell, G.R., Jr., and P. Cornillon, Large-scale variability in the western North Atlantic subtropical convergence zone during FASINEX, Part I, Description of the SST and wind stress fields, *J. Phys. Oceanogr., 20,* 211–222, 1990*a*.

Halliwell, G.R., Jr., and P. Cornillon, Large-scale variability in the western North Atlantic subtropical convergence zone during FASINEX, Part II; Upper ocean heat balance and frontogenesis, *J. Phys. Oceanogr., 20,* 223–234, 1990*b*.

Halliwell, G. R., Jr., P. Cornillon, K. H. Brink, R. T. Pollard, D. L. Evans, L. A. Regier, J. M. Toole, and R. W. Schmidt, Descriptive oceanography during the Frontal Air-Sea Interaction Experiment: Medium to large-scale variability, *J. Geophys. Res.,* this issue.

Levitus, S., Climatological atlas of the world ocean, *NOAA Prof. Pap. 13,* Nat'l Oceanic and Atmos. Admin., Washington, D.C., 1982.

Neumann, G., and W. J. Pierson, *Principles of Physical Oceanography,* 545 pp., Prentice-Hall, Englewood Cliffs, N.J., 1966.

Ramage, C. S., Can shipboard measurements reveal secular changes in tropical air-sea heat flux? *J. Clim. and Appl. Meteorol., 23,* 187–183, 1984.

Ramage, C. S., Secular change in reported surface wind speeds over the ocean, *J. Clim. and Appl. Meteorol., 26,* 525–528, 1987.

Schroeder, E., Average monthly temperatures in the North Atlantic Ocean. *Deep-Sea Res., 12,* 323–343, 1965.

Slutz, R. J., S. J. Lubker, J. D. Hiscox, S. D. Woodruff, R. L. Jenne, D. L. Joseph, P. M. Steuer, and J. D. Elms, Comprehensive ocean-atmosphere data set, Release I, 268 pp., Clim. Res. Div., NOAA Environ. Res. Lab., Boulder, Colo., 1985. (Available as NTIS PB86-105723 from Nat'l. Tech. Inf. Serv., Springfield, Va.)

Smith, S. D., Coefficients for sea surface wind stress, heat flux, and wind profiles as a function of wind speed and temperature, *J. Geophys. Res. (C), 93,* 15,467–15,472, 1988.

Stommel, H., The westward intensification of ocean currents, *Eos Trans. AGU, 99,* 202–206, 1948.

Uda, M. and K. Hasunuma, The eastward subtropical countercurrent in the western North Pacific Ocean, *J. Oceanogr. Soc. Japan., 25,* 201–210, 1969.

Voorhis, A. D., E. H. Schroeder, and A. Leetmaa, The influence of deep mesoscale eddies on the sea surface temperature in the North Atlantic subtropical convergence, *J. Phys. Oceanogr., 6,* 953–961, 1976.

Warren, S. G., C. J. Hahn, J. London, R. M. Chervin, and R. L. Jenne, Global Distribution of total cloud cover and cloud type amounts over the ocean, *NCAR/TN-317+STR,* Nat'l Cent. for Atmos. Res., Boulder, Colo., 1988.

Weller, R. A., Overview of the Frontal Air-Sea Interaction Experiment (FASINEX): A study of air-sea interactions in a region of strong oceanic gradients, *J. Geophys. Res.,* this issue.

Weller, R., D. L. Rudnick, C. C. Eriksen, K. L. Polzin, N.S. Oakey, J.W. Toole, R.M. Schmitt, and R. T. Pollard, Forced ocean response in the Frontal Air-Sea Interaction Experiment, *J. Geophys. Res.,* this issue.

Woodruff, S. D., R. J. Slutz, R. L. Jenne, and P. M. Steurer, A comprehensive ocean-atmosphere data set, *Bull. Am. Meteorol. Soc., 69,* 1239–1250, 1987.

Wright, P. B., Problems in the use of ship observations for the study of interdecadal climate changes, *Mon. Weather Rev., 114,* 1028–1034, 1986.

Yoshida, K. and T. Kidokoro, A subtropical counter-current in the North Pacific, *J. Oceanogr. Soc. Japan, 23,* 88–91, 1967.

P. Cornillon, Graduate School of Oceanography, University of Rhode Island, Kingston, RI 02881.

G. R. Halliwell, Jr., and V. Halliwell, Division of Meteorology and Physical Oceanography, Rosenstiel School of Marine and Atmospheric Science, University of Miami, 4600 Rickenbacker Causeway, Miami, FL 33149.

H. P. Hanson (corresponding author), Atmospheric and Climate Dynamics Program, Cooperative Institute for Research in Environmental Sciences, University of Colorado, Boulder, CO 80309-0216.

(Received May 30, 1990;
revised November 13, 1990;
accepted November 13, 1990.)